

Antiferromagnetic Invar and anti-Invar in Fe-Mn alloys

T. Schneider, M. Acet, B. Rellinghaus, E. F. Wassermann, and W. Pepperhoff

Tiefemperaturphysik (SFB 166), Gerhard-Mercator-Universität Duisburg, 47048 Duisburg, Germany

(Received 24 August 1994)

We present measurements of the thermal-expansion coefficient $\alpha(T)$ on $\text{Fe}_{100-x}\text{Mn}_x$ alloys with $15 < x < 60$ at. % in the temperature range $4 < T < 1150$ K. The results show that $\alpha(T)$ is anomalously enhanced especially in the high-temperature range. The total volume expansion between 0 K and the melting point T_m is up to 70% larger as compared to the volume expansion of a normal metal in the range $0 < T < T_m$. A similar enhancement has earlier been found in fcc Fe and is referred to as the anti-Invar effect. An analysis is presented in order to determine the quantitative anti-Invar contribution to $\alpha(T)$ in Fe-Mn. The observed behavior is discussed in terms of moment-volume instabilities, which are known to be responsible for the Invar effect.

I. INTRODUCTION

Magnetic fcc $3d$ alloys within certain electron concentrations per atom e/a exhibit the Invar effect, i.e., a reduced thermal-expansion coefficient $\alpha(T)$ in comparison to that of a Grüneisen lattice.^{1,2} The effect is observed in ferromagnetic (FM) alloys ($8.5 < e/a < 9$) for $T < T_c$ as well as in antiferromagnetic (AF) alloys ($7.3 < e/a < 7.8$) for $T < T_N$, and is called FM Invar and AF Invar, respectively. On the other hand, fcc $3d$ alloys with $e/a < 8.5$ in the paramagnetic (PM) state have an $\alpha(T)$ which is larger than that described by a Grüneisen lattice.^{3,4} This is referred to as anti-Invar behavior. It is also a property of elemental fcc Fe (Ref. 5) and fcc Mn.^{6,7} Both the reduced $\alpha(T)$ of FM and AF Invar and the enhanced $\alpha(T)$ of anti-Invar are caused by moment-volume instabilities (MVI's).^{1,5,8} Total-energy calculations as a function of moment and volume $E(M, V)$ reveal that in FM Invar (e.g., $\text{Fe}_{100-x}\text{Ni}_x$) and AF Invar (e.g., ordered Fe-Mn) there is an energetic distortion in the $E(M, V)$ surfaces in the direction of smaller volumes and moments with respect to the ground state (called "reduced anharmonicity").^{9,10} In anti-Invar, which is the subject of recent theoretical research [e.g., fcc Fe (Refs. 11–14)], the effect is in the opposite direction, i.e., the distortion is in the direction of larger volumes and increasing moments with respect to the ground state ("enhanced anharmonicity").

fcc $\text{Fe}_{100-x}\text{Mn}_x$ alloys in the concentration range $30 < x < 60$ at. % show AF Invar properties.^{15,16} On the other hand, with fcc Fe and fcc Mn as anti-Invar components, fcc Fe-Mn alloys are also expected to show anti-Invar properties in their corresponding paramagnetic states. However, the existing data^{15,16} of $\alpha(T)$ on fcc Fe-Mn are restricted to temperatures below 700 K, which is too low for identifying the anti-Invar effect in these alloys. Therefore, in the present work, we measured $\alpha(T)$ of $\text{Fe}_{100-x}\text{Mn}_x$ up to 1150 K. The results clearly show the enhanced nature of $\alpha(T)$ in the PM range and thus the anti-Invar effect. Quantitative estimates of the volume increase through this effect will be given.

II. EXPERIMENT

$\text{Fe}_{100-x}\text{Mn}_x$ samples with $x = 15, 25, 30, 40, 50,$ and 60 at. % are prepared by inductive melting in argon atmosphere. The thermal expansion is measured by means of two capacitive dilatometers, one with a copper capacitance cell operating in the temperature range $4.2 < T < 300$ K, the other with a quartz push-rod capacitance cell operating in the range $260 < T < 1150$ K. The thermal-expansion coefficient α is calculated from the relative length change measured in temperature intervals of 5 K.

III. RESULTS AND DISCUSSION

The results of the measurements are shown in Fig. 1, where the thermal-expansion coefficient α is plotted versus the temperature for fcc $\text{Fe}_{100-x}\text{Mn}_x$ alloys with different x . For a better representation, curves have been shifted as indicated in the figure. Data for two alloys with $x = 15$ and 25 (right-hand scale in the figure) are shown only within their corresponding fcc stability range, because they undergo a martensitic transformation at lower temperatures. The arrows mark the Néel temperatures T_N .^{17,18} The overall $\alpha(T)$ behavior with the strong decrease around the ordering temperature is Invar typical; it represents the AF Invar effect.

Conventionally, the Invar contribution to $\alpha(T)$ is determined by subtracting the lattice thermal-expansion coefficient $\alpha_{\text{lat}}(T)$ as calculated from a Grüneisen analysis from the experimental curve $\alpha_{\text{expt}}(T)$. The area between $\alpha_{\text{lat}}(T)$ and $\alpha_{\text{expt}}(T)$ is then equivalent to the spontaneous length magnetostriction λ_s . For a cubic lattice λ_s is related to ω_s , the spontaneous volume magnetostriction, by $3\lambda_s = \omega_s \equiv (\Delta V/V)_s$. $\alpha_{\text{lat}}(T)$ is given by

$$\alpha_{\text{lat}}(T) = \frac{1}{3} \frac{c_v(T)}{Q[1 - KU(T)/Q]^2}, \quad (1)$$

where $c_v(T)$ is the Debye specific heat at constant volume and $U(T)$ is the internal energy. K and Q , which are

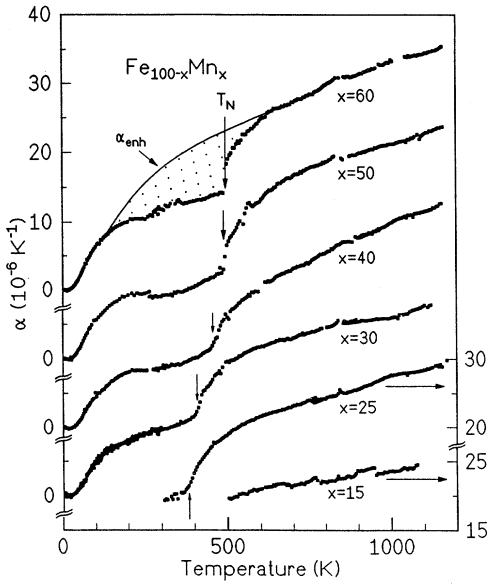


FIG. 1. Thermal-expansion coefficient α versus the temperature T for fcc $\text{Fe}_{100-x}\text{Mn}_x$ alloys with different x . The curves are shifted for clarity. Arrows mark the Néel temperatures T_N . Data for the alloys with $x = 15$ and 25 (right-hand scale), which undergo a martensitic transformation, are shown only in their corresponding fcc stability ranges. The full curve $\alpha_{\text{enh}}(T)$ for the sample with $x = 60$ is a free-hand-drawn curve, connecting low- and high-temperature data. The volume enhancement, proportional to the dotted area, corresponds to the AF Invar effect.

constants related to the interatomic potential and to the Grüneisen parameter, respectively, can be determined from a fit of $\alpha_{\text{lat}}(T)$ [Eq. (1)] to the experimental high-temperature data. In FM Invar alloys this kind of analysis works well for $T > T_c$, because the Invar anomaly has vanished, and the expansion is Grüneisen-like. However, for the present Fe-Mn alloys such an analysis is not reasonable, because the anomalously large thermal-expansion coefficients ($\alpha > 25 \times 10^{-6} \text{ K}^{-1}$) in the PM range lead to unrealistic Grüneisen parameters. Furthermore, the high-temperature data for $T > T_N$ exhibit convex curvatures, not allowing for an accurate fit of $\alpha_{\text{expt}}(T)$ to $\alpha_{\text{lat}}(T)$ given by Eq. (1). Therefore, as defined in the literature,^{15,16} λ_s originating from the AF Invar effect is identified with the area lying between $\alpha_{\text{expt}}(T)$ and a free-hand drawn curve which smoothly joins the high- and the low-temperature data. An example is shown in Fig. 1 for $x = 60$ (dotted area). We refer to this free-hand-drawn curve as the enhanced reference curve and denote it by $\alpha_{\text{enh}}(T)$.

To find a physically founded reference curve describing the anomalously large high-temperature values of $\alpha(T)$ of Fe-Mn, we note that the absolute value of $\alpha_{\text{lat}}(T)$ of a normal metal at half the melting temperature T_m is given by the empirical relation¹⁹

$$T_m \alpha_{\text{lat}} \left(\frac{T_m}{2} \right) \approx 0.025. \quad (2)$$

Furthermore, the relative volume increase $\Delta V/V$ between 0 K and T_m of such a metal is about 7% and is given also empirically by¹⁹

$$\begin{aligned} \left(\frac{\Delta V}{V} \right)_{\text{lat}} &= 3 \int_0^{T_m} \alpha_{\text{lat}}(T) dT \\ &= 3 \int_0^1 T_m \alpha_{\text{lat}}(T/T_m) d(T/T_m) \approx 0.07. \end{aligned} \quad (3)$$

The background of these two relations is the experimental observation that for all normal metals the relative average displacement of the atoms from their equilibrium positions at the melting point is about 2.3% (Lindemann criterion). In spite of the lack of a theoretical understanding of this observation, we use Eqs. (2) and (3) to find a reference curve for the thermal expansion of anti-Invar. For this purpose we plot in Fig. 2 available thermal-expansion data for normal fcc elements¹⁹ (e.g., Cu, Ni, and Pd) in the form of $T_m \alpha$ as a function of (T/T_m) . As expected from Eqs. (2) and (3), all data lie closely together, and thus can be described by an average curve, representing the general expansion behavior of the lattice of normal fcc metals. We use this average curve, shown in Fig. 2 by the dashed line, as a new reference curve and refer to it as the general lattice expansion curve $T_m \alpha_{\text{lat}}(T)$.

In Fig. 2 we have also plotted $T_m \alpha$ of two of the presently measured Fe-Mn alloys versus T/T_m . One can

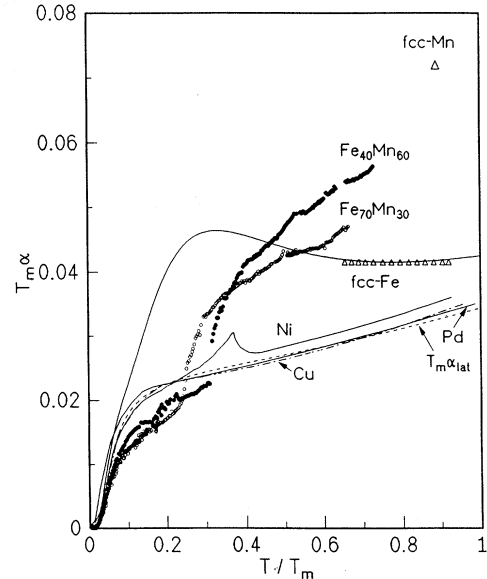


FIG. 2. Product of the melting temperatures T_m and the thermal-expansion coefficients α versus the reduced temperature (T/T_m) for different fcc elements (Pd, Cu, Ni) (Ref. 19). The dashed curve, labeled $T_m \alpha_{\text{lat}}$, represents the average thermal-expansion curve of these elements. Note in comparison the strongly enhanced thermal expansions of two of the presently investigated fcc $\text{Fe}_{100-x}\text{Mn}_x$ alloys with $x = 30$ and 60 and in fcc Fe, for which the calculated (full) curve and the experimental data points (open triangles) are shown in the stability range (Ref. 5). The enhanced thermal expansion in Fe-Mn and fcc Fe is called the anti-Invar effect.

see that in the PM range the data lie far above the general lattice curve $T_m \alpha_{\text{lat}}(T)$. The difference between the experimental data and the general lattice curve for the Fe-Mn alloys is the additional contribution to $\alpha(T)$ originating from the anti-Invar effect. Since the enhancement of the thermal expansion earlier found in fcc Fe has been identified also as an anti-Invar contribution,⁵ we show its $T_m \alpha$ curve in Fig. 2 (open triangles in the fcc stability range). Obviously, the maximum in $T_m \alpha$ originating from the anti-Invar effect found at $T/T_m \approx 0.25$ in fcc Fe is shifted to higher temperatures in the Fe-Mn alloys.

To separate the contributions to $\alpha(T)$ originating from the anti-Invar and the AF Invar effects in Fe-Mn we plot in Figs. 3(a) and 3(b) the experimental data $T_m \alpha_{\text{expt}}(T/T_m)$ for $x = 30$ together with the general lattice curve $T_m \alpha_{\text{lat}}(T)$ (full curve) as taken from Fig. 2. T_N in these plots is shown by the arrows at T_N/T_m . $T_m \alpha_{\text{expt}}(T)$ is the sum of three contributions and is given by

$$T_m \alpha_{\text{expt}}(T) = T_m \alpha_{\text{lat}}(T) + T_m \alpha_{\text{anti-Invar}}(T) + T_m \alpha_{\text{AF Invar}}(T). \quad (4)$$

$T_m \alpha_{\text{AF Invar}}(T)$ denotes the contribution from the AF Invar effect which we assume to vanish at temperatures well above T_N , as in FM Invar for $T > T_c$. $T_m \alpha_{\text{anti-Invar}}(T)$ denotes the anti-Invar contribution. For the quantitative determination of these contributions we have two possibilities. The assumption that the anti-Invar effect occurs only in the PM temperature range leads to the result shown in Fig. 3(a). The hatched area above T_N represents the enhanced length change associated with the anti-Invar effect. The dotted area below T_N is the magnetostriction λ_s , associated with the AF Invar effect. The lower part of Fig. 3(a) is a plot of the difference $T_m \Delta\alpha = T_m (\alpha_{\text{expt}} - \alpha_{\text{lat}})$.

Since there are no finite-temperature calculations describing the thermal behavior of the anti-Invar contribution, we do not know whether the anti-Invar effect starts at T_N or is already present at $T < T_N$. Therefore a second way to analyze our data is to assume that the anti-Invar effect starts at $T = 0$. In this manner, anti-Invar and AF Invar contributions superpose in the range $T < T_N$. The sum of $T_m \alpha_{\text{lat}}(T)$ and $T_m \alpha_{\text{anti-Invar}}(T)$, as shown in Fig. 3(b), is then the enhanced reference curve $T_m \alpha_{\text{enh}}(T)$. The hatched area between $T_m \alpha_{\text{enh}}(T)$ and $T_m \alpha_{\text{lat}}(T)$ is the length change associated with the anti-Invar effect and the dotted area between $T_m \alpha_{\text{enh}}(T)$ and $T_m \alpha_{\text{expt}}(T)$ is the AF Invar contribution. The lower part of Fig. 3(b) is the difference $T_m \Delta\alpha$ as given above. λ_s now is somewhat larger than in the analysis in Fig. 3(a). The curve $\alpha_{\text{enh}}(T)$ has been used in earlier publications^{15,16} as a reference to determine the AF Invar contribution.

From our experimental data we cannot decide whether the anti-Invar effect appears in the total temperature range $0 < T < T_m$ or starts to contribute to $\alpha(T)$ at $T > T_N$. The answer must be left open until finite-temperature band-structure calculations give at least an indication where the anti-Invar behavior is supposed to

start. A comparison with pure fcc Fe is not suitable either, since the Néel temperature $T_N = 68$ K is too low to allow for a conclusive comparison.

The total volume enhancement due to the anti-Invar

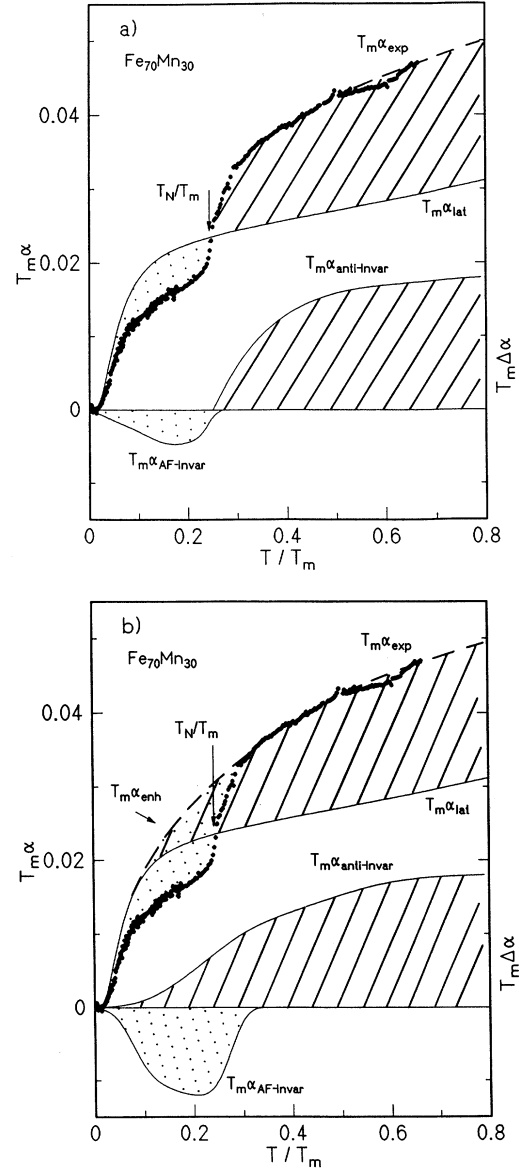


FIG. 3. Plots of $T_m \alpha$ versus (T/T_m) showing two possible ways of determining the different contributions from AF Invar and anti-Invar to the thermal expansion of $\text{Fe}_{70}\text{Mn}_{30}$ (full points). (a) The two effects occur separately; AF Invar (dotted area) in the range $0 < T < T_N$, anti-Invar (hatched area) in the PM range for $T_N < T < T_m$. $T_m \alpha_{\text{lat}}$ (full curve) is the general lattice curve as determined in Fig. 2. The lower plot gives the difference $T_m \Delta\alpha = T_m (\alpha_{\text{expt}} - \alpha_{\text{lat}})$. (b) The two effects superpose in the range below T_N . There are two different reference curves, $T_m \alpha_{\text{enh}}$ (cf. Fig. 1) for determination of the AF Invar contribution (dotted area) and $T_m \alpha_{\text{lat}}$ for determination of the anti-Invar contribution (hatched area). The difference curves are shown in the lower part of (b).

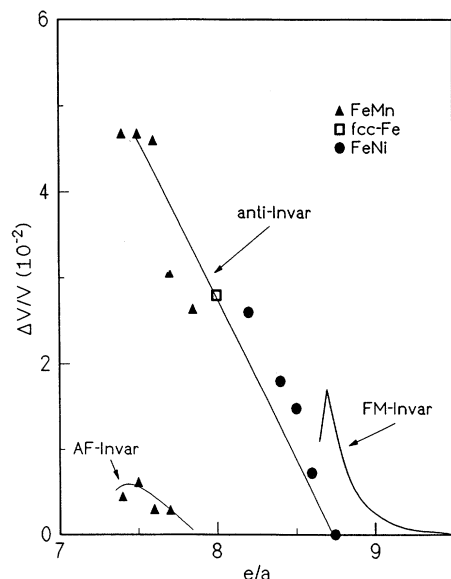


FIG. 4. Relative volume enhancement $\Delta V/V$ versus the electron concentration e/a for different fcc alloys, originating from the FM Invar and AF Invar effects (Ref. 1) and from the anti-Invar effect.

effect in Fe-Mn alloys calculated by the second type of analysis up to the melting point ranges from $3.0\% \pm 0.1\%$ for $x = 30$ to 4.7% for $x = 60$ whereas the AF Invar effect amounts to about 0.8% in all the alloys. The spontaneous volume magnetostriction $\Delta V/V$ in FM Invar and the volume enhancement in anti-Invar as a function of electrons per atom e/a are collected in Fig. 4 for fcc Fe,⁵ Fe-Ni,^{3,13} and Fe-Mn alloys. Note that the relative volume increase due to the anti-Invar effect can be more than twice as large as the volume increase due to the FM Invar effect. This is of practical use in, e.g., bimetals which can be composed of a FM Invar and an anti-Invar component.

IV. CONCLUSIONS

In this work we have shown that the thermal expansion of fcc Fe-Mn alloys is considerably enhanced as compared to the expansion of normal fcc metals. We present a method to find a reference lattice curve for anti-Invar alloys allowing for a quantitative determination of the AF Invar and the anti-Invar contributions to $\alpha(T)$. The largest anti-Invar effect is observed in $\text{Fe}_{40}\text{Mn}_{60}$, which experiences a volume expansion of 12% between $T=0$ and $T=T_m$. This is about 70% more than the expansion of a normal metal in the same range, which amount to $\sim 7\%$.

Recent theoretical and experimental results show that anti-Invar behavior originates from moment-volume instabilities^{5,8} in a similar fashion to the FM Invar effect in alloys like Fe-Ni or Fe-Pt.^{1,2} Previous calculations on ordered Fe-Mn (Refs. 10, 20, 21) did not bring the anti-Invar effect forward. However, calculations which are currently being done suggest that a MVI exists on Fe_3Mn .²² Here, the AF ground state is characterized by an antiparallel coupling of the Mn moments with respect to the Fe moments, while at expanded volumes the moments couple ferromagnetically. This MVI gives rise to an "enhanced anharmonicity" in the total energy $E(M, V)$. The enhanced $\alpha(T)$, as measured on fcc Fe-Mn alloys in the present work, is a direct measure of the enhanced anharmonicity of the alloys and can be regarded as a confirmation of the calculated ground-state properties.

Though first-principles calculations of $\alpha(T)$ at finite temperatures are very recent, the results on Fe-Ni Invar,⁹ Fe-Pt Invar,¹³ and fcc Fe anti-Invar¹³ are promising. For a quantitative comparison between the results of theoretical calculations and experimental data, a reliable method for the determination of Invar and anti-Invar contributions to $\alpha(T)$ is of substantial importance.

ACKNOWLEDGMENTS

This work was supported by Deutsche Forschungsgemeinschaft (SFB 166).

¹E. F. Wassermann, in *Ferromagnetic Materials V*, edited by K. H. J. Buschow and E. P. Wohlfarth (North-Holland, Amsterdam, 1990), p. 240.

²E. F. Wassermann, *J. Magn. Magn. Mater.* **100**, 346 (1991).

³M. Acet, T. Schneider, H. Zähres, E. F. Wassermann, and W. Pepperhoff, *J. Appl. Phys.* **75**, 7015 (1994).

⁴W. Bendick, H. H. Ettwig, and W. Pepperhoff, *J. Phys. F* **8**, 2525 (1978).

⁵M. Acet, H. Zähres, E. F. Wassermann, and W. Pepperhoff, *Phys. Rev. B* **49**, 6012 (1994).

⁶M. Acet, H. Zähres, W. Stamm, E. F. Wassermann, and W. Pepperhoff, *Physica B* **161**, 67 (1989).

⁷M. Acet, T. Schneider, E. F. Wassermann, and W. Pepperhoff, *J. Appl. Phys.* **75**, 7017 (1994).

⁸V. L. Moruzzi, *Phys. Rev. B* **41**, 6939 (1990).

⁹H. Ebert, M. Schröter, G. G. Reddy, P. Entel, E. Hoffmann, and H. Akai (unpublished).

¹⁰M. Podgorny, *Phys. Rev. B* **45**, 797 (1992).

¹¹V. L. Moruzzi, P. M. Marcus, and J. Kübler, *Phys. Rev. B* **39**, 6957 (1989).

¹²M. Uhl, L. M. Sandratskii, and J. Kübler, *J. Magn. Magn. Mater.* **103**, 314 (1992).

¹³M. Uhl, L. M. Sandratskii, and J. Kübler, *Phys. Rev. B* **50**, 291 (1994).

¹⁴E. Hoffmann, P. Entel, K. Schwarz, and P. Mohn (unpublished).

¹⁵H. Fujimori, *J. Phys. Soc. Jpn.* **21**, 1860 (1966).

¹⁶W. Richter and W. Pepperhoff, *Arch. Eisenhüttenwes.* **47**, 45 (1976).

¹⁷ T_N is taken as the temperature corresponding to the peak in c_p . Neutron diffraction studies in Ref. 12 show T_N lying slightly higher.

¹⁸T. Hashimoto and Y. Ishikawa, *J. Phys. Soc. Jpn.* **23**, 213 (1967).

¹⁹Y. S. Touloukian, R. K. Kirby, R. E. Taylor, and P. D. Desai, *Thermal Expansion*, Thermophysical Properties of Matter Vol. 12 (IFI/Plenum, New York, 1977). The present values used in Eqs. (2) and (3) are improved ones, and therefore slightly different from this reference.

²⁰J. Kübler, K.-H. Höck, J. Sticht, and A. R. Williams, *J. Phys. F* **18**, 469 (1988).

²¹O. Jepsen and F. Herman, *Phys. Rev. B* **41**, 6801 (1990).

²²E. Hoffmann and P. Entel (unpublished).